An Observational Study of the Intraseasonal Poleward Propagation of Zonal Mean Flow Anomalies

STEVEN B. FELDSTEIN

Earth System Science Center, The Pennsylvania State University, University Park, Pennsylvania

ABSTRACT

The poleward propagation of zonal-mean relative angular momentum (M_R) anomalies is examined using NCEP–NCAR Reanalysis data for both the winter and summer seasons of the Northern and Southern Hemisphere. This analysis is performed with a regression analysis using base latitudes in the subtropics, midlatitudes, and high latitudes. It is found that the poleward M_R anomaly propagation occurs at all latitudes, with the propagation speed being greater in the subtropics and high latitudes, compared to midlatitudes.

Other fields, such as eddy angular momentum flux convergence, eddy heat flux, friction torque, and 300-mb streamfunction, are regressed for the Northern Hemisphere winter and the Southern Hemisphere summer. The main finding is that in the subtropics and midlatitudes, the poleward M_R anomaly propagation is primarily due to high-frequency (<10 day) transient eddy angular momentum flux convergence and in high latitudes the propagation is mostly due to the summation of cross-frequency and low-frequency (>10 day) eddy angular momentum flux convergence. For the Northern Hemisphere winter, the anomalous eddy angular momentum flux convergence due to the interaction between stationary and transient eddies also contributes to the poleward M_R anomaly propagation.

The regression analysis suggests that a high-frequency transient eddy feedback is taking place that influences the poleward propagation of the M_R anomalies. However, the effectiveness of this feedback is limited by the summation of the cross-frequency and low-frequency eddy angular momentum flux convergence, as once the M_R anomaly reaches its largest amplitude, this summation of terms dominates the eddy angular momentum flux convergence and, together with the friction torque, contributes to the decay of the M_R anomaly.

1. Introduction

For the past several decades, there has been a tremendous research effort toward both observing and understanding the properties of the *climatological* zonally averaged flow. One of the primary motivations for the extensive research on this subject is that the zonally averaged flow is known to have a major influence on both transient and stationary eddies, which in turn has important consequences for both local weather and climate. In contrast, research on the *temporal variation* of the zonally averaged flow has been a subject of more recent interest. Most of the earliest investigations tended to concentrate on the zonally averaged flow changes that accompanied idealized baroclinic life cycles (e.g., Pedlosky 1970; Simmons and Hoskins 1978). It has been only within the past 15 years that a number of researchers have been examining the intraseasonal temporal variation of the observed zonally averaged flow (e.g., Kidson 1985, 1986, 1988; Nigam 1990; Karoly 1990;

Lyons and Hundermark 1992; Hartmann 1995). Additional insight into the fundamental dynamics of the temporal variation of the zonally averaged flow has come from several more recent idealized modeling studies (e.g., Yu and Hartmann 1993; Robinson 1991, 1996; Feldstein and Lee 1996; Lee and Feldstein 1996).

The above studies focus on zonally averaged flow anomalies that are spatially fixed. This is most often performed with empirical orthogonal function analysis (Kutzbach 1967). In a recent modeling study, James et al. (1994) found episodes of low-frequency (a typical period of 150 days), equivalent barotropic, poleward-propagating zonal mean zonal wind anomalies. However, their model was very idealized, that is, low resolution (triangular truncation at zonal wavenumber 21), five levels, no orography or land–sea contrast, no direct accounting for moist processes, no seasonal cycle, and radiation parameterized as simple Newtonian heating. Nevertheless, the results of James et al. (1994) lead to the interesting question of whether poleward-propagating zonal mean anomalies do occur in the atmosphere. In fact, the observational study of Riehl et al. (1950) provides some evidence for poleward-propagating zonal mean zonal wind anomalies. However, the length of their time series is limited to just 7 months, and their zonal mean is confined to a band of 270° longitude.

Corresponding author address: Dr. Steven B. Feldstein, Earth System Science Center, The Pennsylvania State University, 248 Deike Building, University Park, PA 16802.
E-mail: sbf@essc.psu.edu

The primary aim of this study is to bring to the attention of the atmospheric science community that poleward-propagating zonal mean anomalies are not limited to idealized models (e.g., James et al. 1994), but they are indeed a prominent form of intraseasonal variability in the atmosphere. An examination of possible dynamical mechanisms that may account for the poleward anomaly propagation, such as that proposed by James and Dodd (1996), is beyond the scope of this study. However, the diagnostics presented in this study will hopefully provide important clues for future research on the poleward-propagating anomalies.

The data and methodology are presented in section 2. This is followed by the results in section 3 and concluding remarks in section 4.

2. Data and methodology

This study uses daily (0000 UTC) National Centers for Environmental Prediction–National Center for Atmospheric Research (NCEP–NCAR) Reanalysis data that extends from 1 January 1979 to 31 December 1995. As the zonal mean anomalies[1] (in this study, the term anomaly will refer to a deviation from the seasonal cycle) will be expressed in terms of the zonally and vertically integrated relative angular momentum (M_R, hereafter), it is convenient to use sigma coordinates, that is,

$$M_R = \frac{a^2}{g} \int_0^{2\pi} \int_0^1 p_s u \, \cos^2\theta \, d\sigma \, d\lambda, \qquad (1)$$

where u and p_s denote the zonal wind and surface pressure, respectively; σ, λ, and θ the vertical, longitudinal, and latitudinal coordinates; t time; a the earth's radius; and g the gravitational acceleration. The anomalous M_R is integrated over equal latitude bands of 2.25°, and all 28 of the NCEP–NCAR Reanalysis model levels are used. These extend from $\sigma = 0.995$ to $\sigma = 0.0027$. As the aim of this study is to examine poleward propagation of tropospheric zonal mean anomalies, one may question why the vertical integral is not limited to the troposphere. However, it is found that the stratospheric mass is sufficiently small that all the anomaly fields presented in this study are essentially identical whether or not the vertical integral includes the stratosphere (this point will be returned to in section 3a). Furthermore, an advantage with including stratospheric M_R is that the equation for the conservation of M_R is simpler. The horizontal resolution of all fields examined in this study corresponds to a rhomboidal truncation at zonal wavenumber 30.

The poleward propagation of the zonal mean anomalies will be identified by regressing M_R at all latitudes

---

[1] The regression results presented in this study are very similar whether M_R or zonal mean zonal wind is used. The primary differences involve the cosine of latitude squared factor in M_R, which results in regressed values having relatively larger (smaller) values in low (high) latitudes.

against M_R at three base latitudes. In the regression equation, the amplitude of the M_R anomaly at the base latitude is always chosen as one standard deviation. This regression is performed at lags between plus and minus 30 days, for both hemispheres, and for each of the two seasons, defined as November through March and May through September. In this study, these seasons will be referred to as Northern Hemisphere (NH) winter and Southern Hemisphere (SH) summer, and NH summer and SH winter, respectively. Three base latitudes are selected for the regression analysis of either hemisphere: 22.5°, 45.0°, and 66.5°N in the NH, and 22.5°, 45.0°, and 66.5°S in the SH. These three base latitudes will be referred to as subtropical, midlatitude, and high latitude, respectively. (Base points near the equator are not shown, as these base points are highly correlated with globally integrated M_R and reveal very different spatial patterns for the regressed fields. This will be discussed in more detail in section 3a.) The selection of the latitudinal range of these base latitudes was based on the observation that the propagation of dipole and tripole M_R anomalies is most apparent between 15° and 70° latitude for both hemispheres and seasons (this will be shown in section 3a). Furthermore, for each season and hemisphere, it was found that the three base latitudes could sufficiently describe the manner in which M_R anomaly propagation varies with latitude. This is because analyses with intermediate base latitudes reveal a gradual transition in M_R anomaly propagation characteristics between the above three base latitudes. The regression calculations are performed separately for each of the 17 yr in the dataset, and the resulting fields are time averaged.

The equation for the conservation of M_R can be written as

$$\frac{\partial M_R}{\partial t} = -\frac{1}{\cos\theta} \int_0^{2\pi} \int_0^1 \frac{\partial}{\partial\theta} \left(\frac{up_s v \, \cos^2\theta}{g} \right) a \, \cos\theta \, d\sigma \, d\lambda$$

$$+ \, T_F + T_M + T_C + T_G, \qquad (2)$$

where v is the meridional wind, T_F the friction torque, T_M the mountain torque, T_C the Coriolis torque (see Weickmann and Sardeshmukh 1994), and T_G the gravity wave drag torque. This equation relates the tendency of M_R to the sum of the angular momentum flux $[up_s v]$ convergence (the square brackets denote a vertical and zonal integration) and the various torques T_F, T_M, T_C, and T_G, which can be expressed as

$$T_F = a \cos\theta \int_0^{2\pi} \tau_\lambda a \, \cos\theta \, d\lambda,$$

$$T_M = -a \cos\theta \int_0^{2\pi} p_s \frac{\partial h}{\partial\lambda} \, d\lambda,$$

$$T_C = af \cos\theta \int_0^{2\pi} \int_0^1 v \, d\sigma \, d\lambda, \qquad (3)$$

where f is the Coriolis parameter. The expression for T_G, which is more complex, is not indicated. The sign convention adopted for the surface stress τ_λ is such that a positive τ_λ implies a transfer of angular momentum from the solid earth to the atmosphere.

The angular momentum flux $[u p_s v]$, where $[\cdot]$ indicates zonal average, is further separated into its eddy and mean meridional components, that is,

$$[u p_s v] = [u^*(p_s v)^*] + [u][p_s v], \qquad (4)$$

respectively, where * denotes a deviation from the zonal mean.

Anomalies for each of the terms on the rhs (right-hand side) of (2) are defined as deviations from the seasonal cycle. In this study, for all quantities, the seasonal cycle is obtained by calculating the time mean value for each calendar day, followed by a smoothing with a 20-day low-pass digital filter. The results to be presented in this study are insensitive to the manner in which the seasonal cycle is smoothed.

The spatial and temporal structure for each of the anomalous flux convergences and torques is obtained by regression against M_R at the three base latitudes in either hemisphere. The amplitude of the M_R anomalies at these base latitudes is again one standard deviation. As the anomalous eddy angular momentum flux convergence and anomalous friction torque are the dominant terms on the rhs of (2) (in general, for most cases analyzed in this study, the maximum anomalous eddy angular momentum flux convergence is typically twice the magnitude of the maximum anomalous friction torque, about five times greater than the maximum anomalous mountain torque, and about ten times greater than the maximum anomalous Coriolis and gravity wave drag torques), only the regressed fields for these two quantities will be presented. Further insight into the characteristics of the poleward M_R anomaly propagation will be obtained by examining regressions of the anomalous zonally averaged eddy heat flux and the anomalous 300-mb streamfunction.

The M_R, friction torque, and 300-mb streamfunction anomaly fields presented in this study will remain temporally unfiltered. On the other hand, both unfiltered and filtered eddy angular momentum fluxes will be shown. This temporal decomposition is obtained by separating u^* and $(p_s v)^*$ into contributions from high-frequency transient eddies (period less than 10 days), low-frequency transient eddies (period greater than 10 days), and stationary eddies (climatological seasonal mean eddies). The low-frequency eddies are defined relative to the climatological seasonal mean. The filtering is accomplished with a 31-point digital filter. Applying this decomposition, with u^* and $(p_s v)^*$ each written as a sum of their high-frequency, low-frequency, and stationary components, yields the following expression for the eddy angular momentum flux

$$
\begin{aligned}
[u^*(p_s v)^*] &= [u_M^*(p_s v)_M^*] + [u_M^*(p_s v)_L^*] + [u_M^*(p_s v)_H^*] \\
&+ [u_L^*(p_s v)_M^*] + [u_H^*(p_s v)_M^*] + [u_H^*(p_s v)_H^*] \\
&+ [u_H^*(p_s v)_L^*] + [u_L^*(p_s v)_H^*] + [u_L^*(p_s v)_L^*],
\end{aligned}
\qquad (5)
$$

where the subscripts M, L, and H denote stationary, low-frequency, and high-frequency, respectively. This expression allows us to determine the relative roles of the stationary–transient interaction [the second through fifth terms on the rhs of (5), referred to as the linear terms, hereafter] and the transient–transient interaction [the last four terms on the rhs of (5)]. An analogous expression can be derived for the mean meridional angular momentum flux.

For all quantities presented, statistical significance is determined using cross-correlation fields, with the number of degrees of freedom, NDOF, being estimated with the procedure in Davis (1976), where

$$\mathrm{NDOF} = N \delta t / \tau, \qquad (6)$$

$$\tau = \sum_k C_x(k \delta t) C_y(k \delta t) \delta t, \qquad (7)$$

N is the number of days in the timeseries, δt the time interval between successive values, that is, one day, and C_x and C_y the autocorrelations of the base and regressed timeseries, respectively. At most latitudes and for most fields in this study, it is found that NDOF is well in excess of 200.

3. Results

a. Meridional propagation

Before presenting the linearly regressed M_R fields, two examples of poleward M_R anomaly propagation are presented in the form of latitude–time diagrams. One example is for the NH winter of 1991–92 (Fig. 1a), and the other for the SH summer of 1990–91 (Fig. 1b). In this figure, time begins on 1 November and continues through the season. Both examples show particularly coherent dipole and tripole poleward M_R anomaly propagation. A closer examination of Figs. 1a and 1b reveals that anomalies of both sign propagate from equatorial regions to a latitude of about 75° and that the anomalies persist for up to half a season, that is, approximately 75 days. Such characteristics are quite similar to the example presented in James et al. (1994) (cf. Fig. 5a of James et al.).

We next objectively diagnose the poleward anomalous M_R propagation by regressing M_R at all latitudes against M_R at the three base latitudes, as described in the previous section. This is presented for the NH winter (summer) in Figs. 2a–c (2d–f) and for the SH winter (summer) in Figs. 3a–c (3d–f). In these figures, the regressed anomalous M_R fields are contoured, and the shading denotes values that exceed the 95% significance level. As in the examples of Fig. 1, the picture that
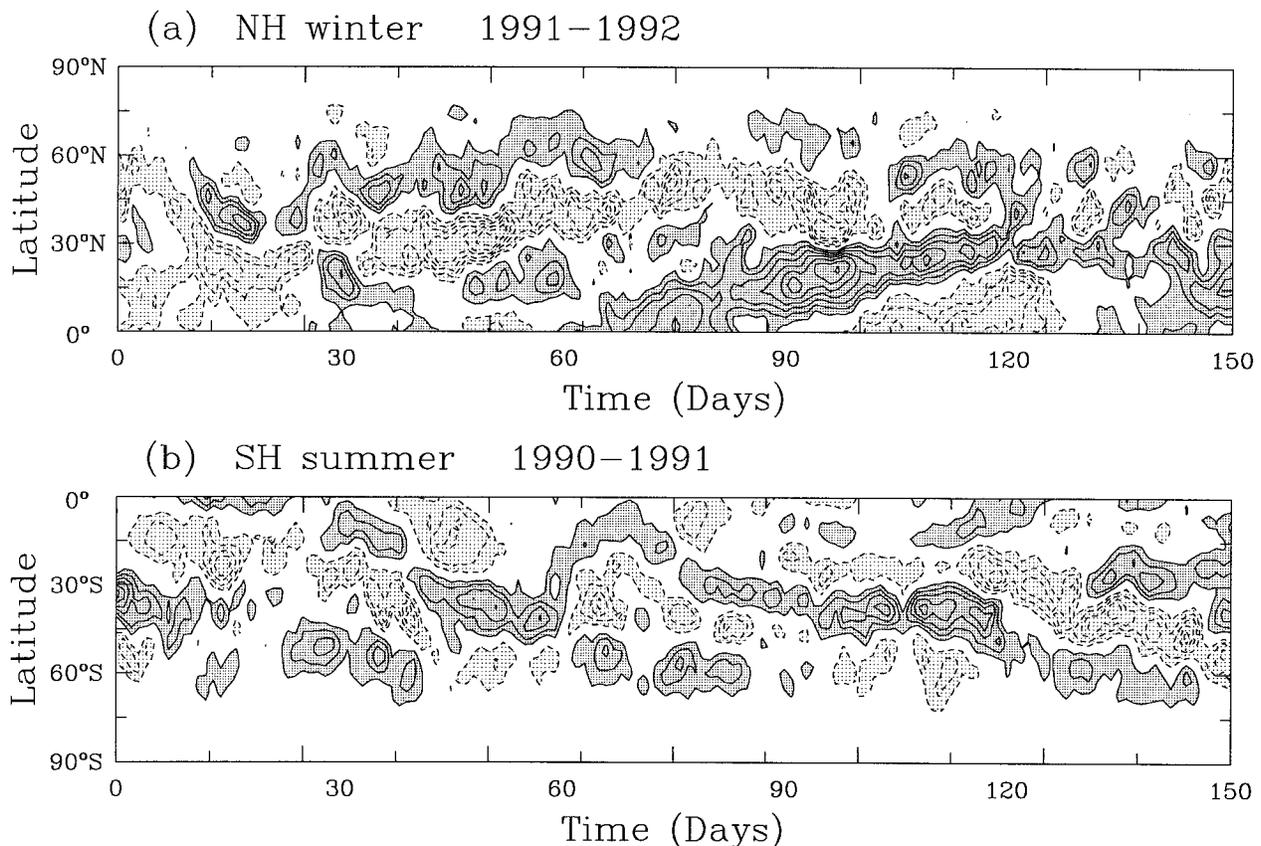
FIG. 1. Latitude–time diagram of anomalous M_R for (a) the NH winter of 1991/92 and (b) SH summer of 1990/91. The contour interval is 0.4×10^{24} kg m^2 s^{-1}. Solid contours are positive, dashed contours negative, and the zero contour is omitted. Shaded values exceed a magnitude of 0.4×10^{24} kg m^2 s^{-1}, with dark (light) shading denoting positive (negative) values.

emerges for each of the above seasons and hemispheres is that poleward propagation of dipole or tripole M_R anomalies is indeed a prominent form of zonal mean flow variability. This propagation is found at all base latitudes with the meridional phase speed of the M_R anomalies being smallest for the midlatitude base latitude. For example, during the SH summer (Figs. 3d–f), the mean poleward propagation speed (averaged between lag -10 and lag $+10$ days for the subtropical and midlatitude base latitudes and between lag -10 days and lag 0 for the high-latitude base latitude) for the subtropical M_R anomaly is approximately $0.53°$ day^{-1}, for the midlatitude anomaly $0.41°$ day^{-1}, and for the high latitude anomaly $0.71°$ day^{-1}. A close examination of the poleward M_R anomaly propagation shows that its speed is least uniform for the midlatitude base latitude, as the propagation speed is close to zero for several days near lag 0. Furthermore, for each season and hemisphere, when the base point is located in high latitudes, the poleward M_R anomaly propagation is followed by equatorward M_R anomaly propagation.

The amount of time that individual anomalies exist is identified as occuring over that time interval for which the signal is statistically significant. However, an ex-

amination of Figs. 2 and 3 reveals that no general statement can be made on the amount of time that individual anomalies can be identified. For example, the subtropical anomalies can be seen to last for approximately 25–40 days, the midlatitude anomalies for 20–30 days, and the high-latitude anomalies for 15–30 days.

In the previous section, it was stated that the stratosphere has a negligible influence on the poleward M_R anomaly propagation. In order to show this quantitatively, a series of linear pattern correlations were generated that involved each of the patterns in Figs. 2 and 3 and the corresponding patterns obtained from a linear regression analysis with the stratosphere excluded (for the latter calculation, the identical procedure to that for Figs. 2 and 3 was used, except that the vertical integral was restricted to between the surface and 200 mb). With the exception of the NH winter high-latitude base latitude, which revealed a correlation of 0.891, all of the other regression maps in Figs. 2 and 3 showed pattern correlations between 0.985 and 0.995, clearly indicating the negligible contribution of the stratosphere to the poleward M_R anomaly propagation.

As stated in section 2, when the base point is located near the equator, the anomalous M_R field takes on a
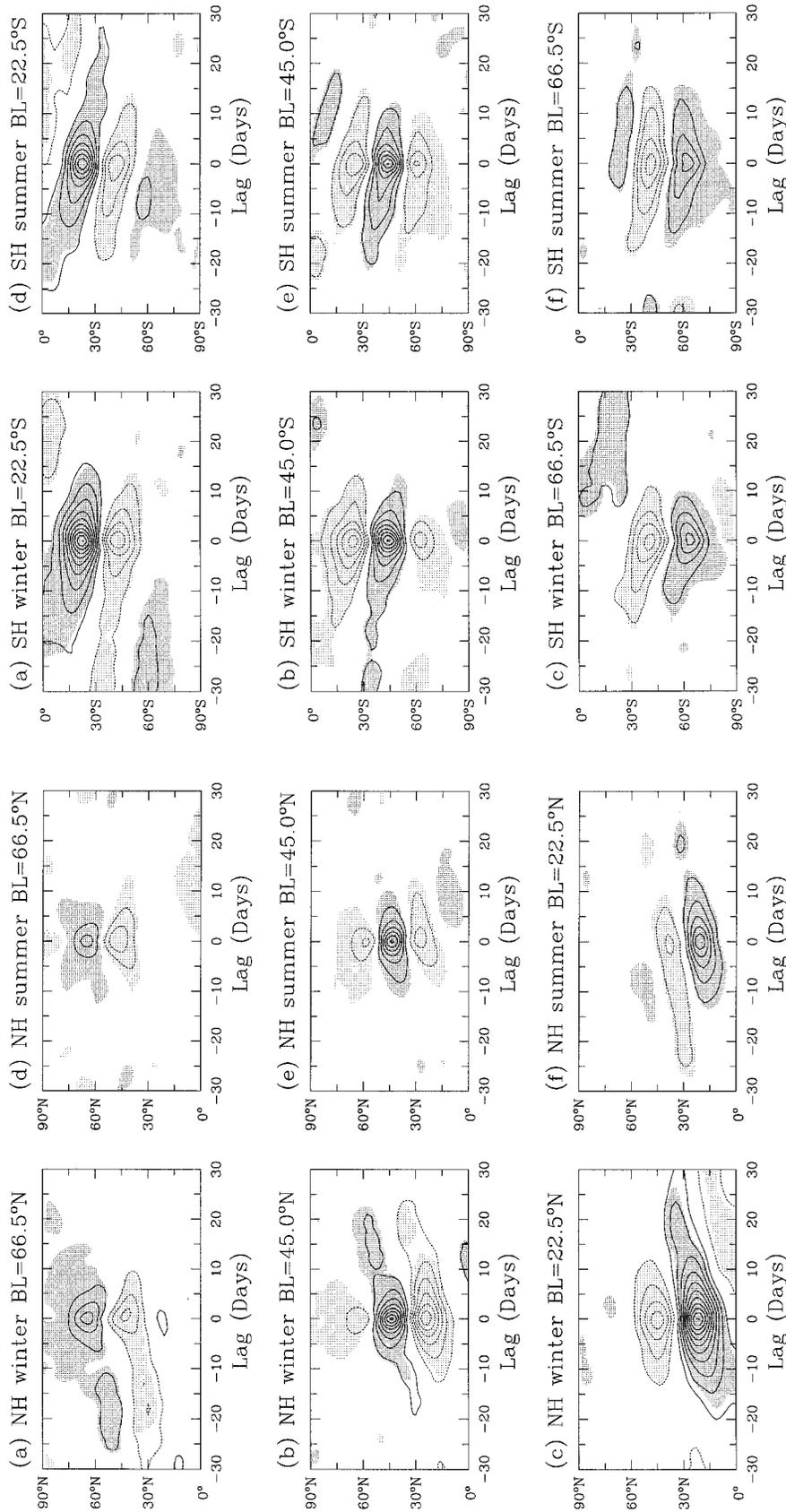
FIG. 2. Regressed NH anomalous M_R as a function of lag and latitude for winter and summer seasons. The symbol BL at the top of each frame denotes the base latitude. The contour interval is 0.1×10^{24} kg m^2 s^{-1}. Solid contours are positive, dashed contours negative, and the zero contour is omitted. Shaded values exceed the 95% significance level, with dark (light) shading denoting positive (negative) t values.

FIG. 3. As Fig. 2, except for the SH.

spatial and temporal structure extremely similar to that found by regression against the globally integrated M_R. When such calculations are performed, propagation of anomalous M_R from the equator to the subtropics is found. At a given lag, the M_R anomalies are mostly of one sign. Such sign properties are distinctly different from the examples presented in Figs. 2 and 3, where the M_R anomalies took on dipole or tripole structures. The above relationship between the poleward propagation of anomalous M_R and globally integrated relative angular momentum has been found in many observational studies, for example, Weickmann et al. (1997).

b. Eddy fluxes and friction torque

The regressed eddy angular momentum flux convergences and friction torques are illustrated for the NH winter and SH summer. These two seasons are selected since they coincide with the two extrema in the stationary wave amplitude, that is, largest (smallest) during the NH winter (SH summer). The anomalous eddy angular momentum flux convergence is shown for the NH winter (SH summer) in Figs. 4a–c (Figs. 5a–c), and the corresponding anomalous friction torque is presented for the NH winter (SH summer) in Figs. 4d–f (Figs. 5d–f). Both of these fields are integrated over equal latitude bands of 2.25°. The most apparent feature in Figs. 4a–c and 5a–c is that the anomalous eddy angular momentum flux convergence has a spatial structure that contributes to amplification of the M_R anomalies (see Figs. 2a–c and 3d–f) before lag 0. Note that the time of the M_R anomaly maximum occurs at lag 0 at the base latitudes. After lag 0, for the subtropical and midlatitude base latitudes, the eddy angular momentum flux convergence anomalies contribute to the decay of the M_R anomalies but are less well organized and exist for a shorter period of time compared to those before lag 0. For the high-latitude base latitude, after lag 0, the anomalous eddy angular momentum flux convergence no longer exhibits much organized structure. The anomalous friction torque, on the other hand, maintains a similar spatial pattern to the M_R anomaly, but of opposite sign, both before and after lag 0. In this manner, the anomalous friction torque is always contributing to the decay of the M_R anomalies.

A close examination of the anomalous eddy angular momentum flux convergence reveals that between 5 and 10 days before lag 0, their extrema typically lie between 2° and 5° poleward of the M_R anomaly extrema, whereas by 5 days after lag 0 (for the subtropical and midlatitude base latitudes), anomalous eddy angular momentum flux convergence extrema, of opposite sign, usually occur about 2°–5° equatorward of the M_R anomaly extrema. It is these spatial differences that must account for the meridional propagation of the M_R anomalies both before and after lag 0. This point will be returned to later in this section.

The decomposition of the anomalous eddy angular momentum flux convergence into different frequency bands, as discussed in section 2, yields greater insight into the properties of these fluxes (Fig. 6). We first examine this decomposition for the SH summer, since the eddy flux properties are simpler to describe during this season, and it is found that the convergence of the linear terms [the second through fifth terms in (5)] is negligible. In Fig. 6, the contours correspond to particular combinations of the anomalous eddy angular momentum flux convergence, and the shading indicates the location of the statistically significant M_R anomalies (the shading is identical to that in Figs. 3d–f). In order to examine the role of the anomalous eddy angular momentum flux convergence in driving the M_R anomalies poleward, we concentrate on the latitudinal phase relationship between these two quantities; a quadrature relationship would indicate that the eddies force a latitudinal acceleration of the M_R anomalies, and an in-phase relationship would reveal that the eddies maintain the M_R anomalies against dissipation. It can be seen that for the subtropical base latitude (Fig. 6a), the anomalous high-frequency (HF, hereafter) [term 6 on the rhs of (5)] eddy angular momentum flux convergence is close to being in spatial quadrature with the anomalous M_R, with the former being poleward of the latter. For the midlatitude base latitude (Fig. 6b), the anomalous HF eddy momentum flux convergence is also poleward of the anomalous M_R, but these two fields are closer to being in phase. For the high-latitude base latitude (Fig. 6c), the anomalous HF eddy momentum flux convergence and anomalous M_R mostly coincide. These spatial phase relationships indicate that the anomalous convergence of the HF eddy angular momentum fluxes contributes primarily to the poleward propagation of the M_R anomalies at subtropical latitudes, to both poleward propagation and growth of the M_R anomalies at midlatitudes, and mostly to just growth of the M_R anomalies at high latitudes.

An entirely different picture is obtained from the summation of the anomalous eddy angular momentum flux convergence associated with the cross-frequency (CF, hereafter) [terms 7 and 8 on the rhs of (5)] and the low-frequency (LF, hereafter) [term 9 on the rhs of (5)] terms, as shown in Figs. 6d–f. We examine the summation of these three terms, rather than showing them separately, as individually these terms all show similar spatial patterns. An examination of the latitudinal phase relationship between the anomalous eddy angular momentum flux convergence and the M_R anomalies reveals that in subtropical and midlatitudes these terms contribute to the growth of the M_R anomalies before lag 0, and to the decay of the M_R anomalies after lag 0, having less influence on the poleward propagation of the M_R anomalies. However, at high latitudes, this summation of terms contributes to both the poleward and equatorward propagation of the M_R anomalies.

The corresponding decomposition of the anomalous eddy angular momentum flux convergence for the NH
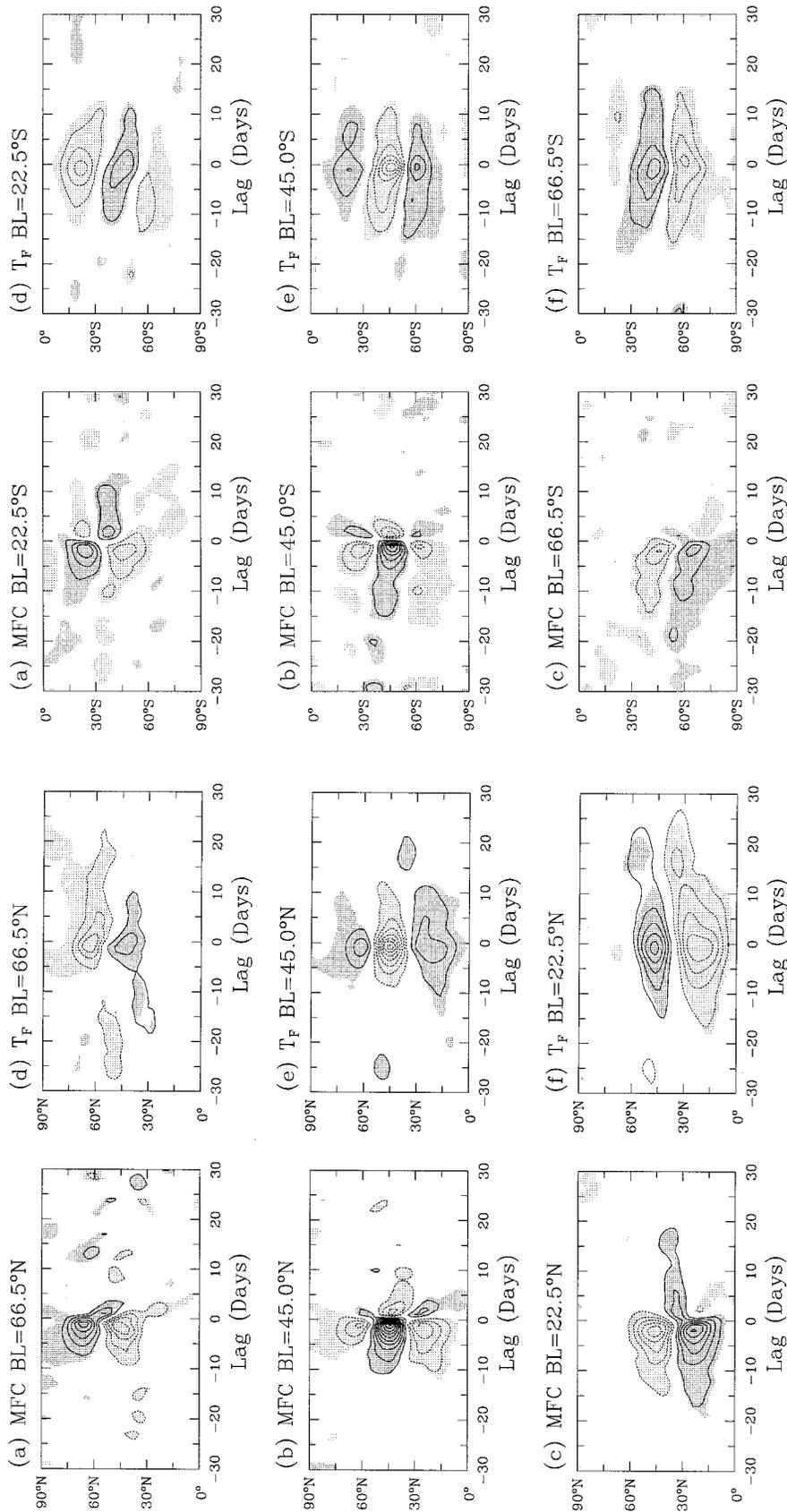
FIG. 4. Regressed anomalous eddy angular momentum flux convergence with base latitudes of (a) 66.5°N, (b) 45.0°N, and (c) 22.5°N, and regressed anomalous friction torque with base latitudes of (d) 66.5°N, (e) 45.0°N, and (f) 22.5°N. The quantities are shown for the NH winter as function of lag and latitude. The contour interval in (a) to (c) is 0.25×10^{18} kg m^2 s^{-2}, and the contour interval in (d) to (f) is 0.125×10^{18} kg m^2 s^{-2}. Solid contours are positive, dashed contours negative, and the zero contour is omitted. Shaded values exceed the 95% significance level, with dark (light) shading denoting positive (negative) t values.

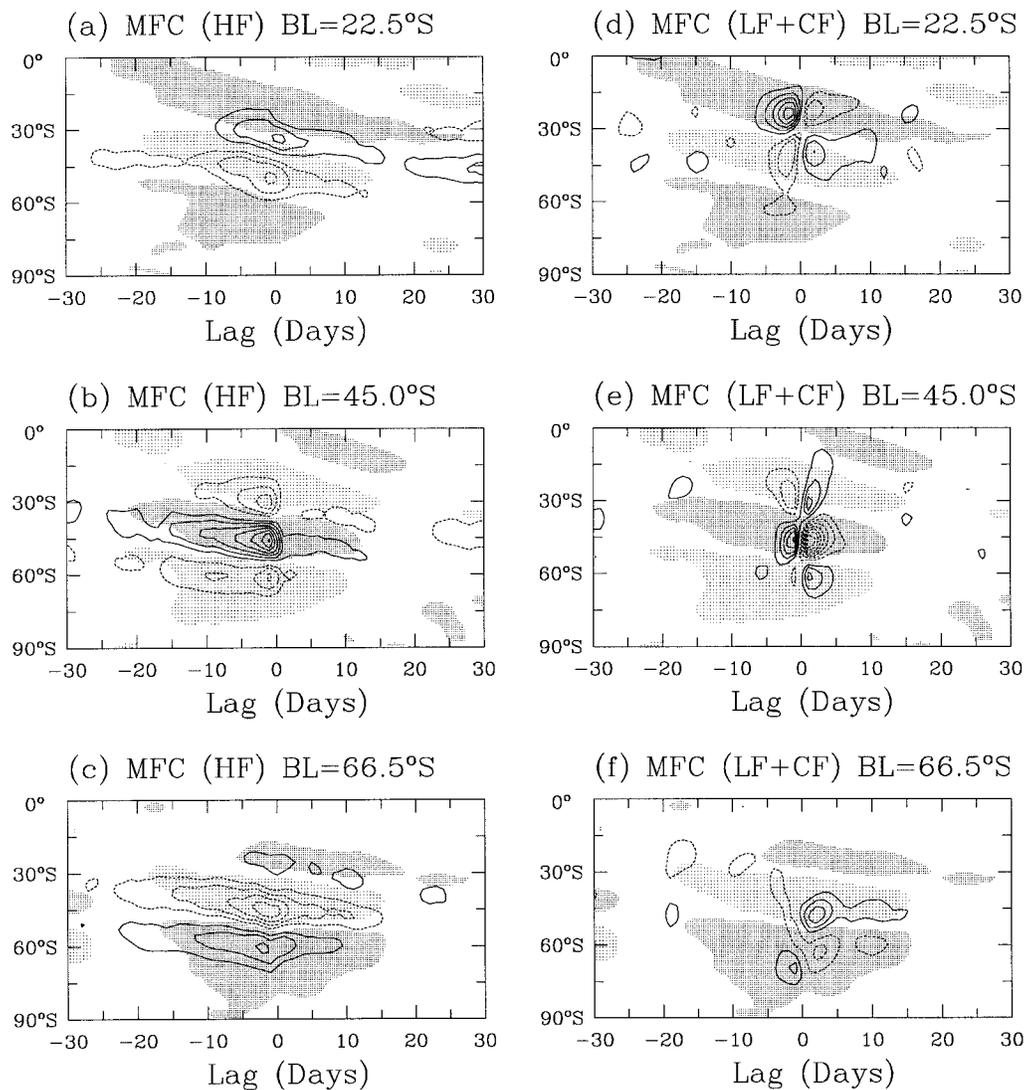FIG. 5. As Fig. 4, except for the SH summer.

FIG. 6. Regressed anomalous HF eddy angular momentum flux convergence with base latitudes of (a) 22.5°S, (b) 45.0°S, and (c) 66.5°S, and regressed anomalous summation of the low-frequency and cross-frequency eddy angular momentum flux convergence terms at (d) 22.5°S, (e) 45.0°S, and (f) 66.5°S. These quantities are shown for the SH summer as function of lag and latitude. The contour interval is 0.125×10^{18} kg m^2 s^{-2}. Solid contours are positive, dashed contours negative, and the zero contour is omitted. Shaded values correspond to the anomalous M_R values that exceed the 95% significance level, with dark (light) shading denoting positive (negative) t values.

winter yields somewhat more complex pictures compared to the SH summer. For example, the subtropical base latitude anomalous HF eddy angular momentum flux convergence is also poleward of the anomalous M_R, but a clear quadrature relationship is not seen (Fig. 7c). For the midlatitude and high-latitude base latitudes, the HF eddy angular momentum flux convergence anomalies coincide with the M_R anomalies (Figs. 7a,b). The anomalous linear eddy angular momentum flux convergence (Figs. 7d–f) also contributes to poleward M_R anomaly propagation, but this is primarily at middle and high latitudes. An examination of the linear terms finds that essentially all of the contribution comes from terms

2 and 4 in (5). Thus, the poleward propagation of the M_R anomalies has contributions from both the HF transient eddies and the interaction between the stationary and LF transient eddies. The analysis of the summation of the anomalous LF and CF eddy angular momentum flux convergence terms (Figs. 7g–i) yields very similar characteristics to that found for the SH summer, as this summation mainly contributes to the growth (decay) of the subtropical and midlatitude M_R anomalies before (after) lag 0 and to the poleward (equatorward) M_R anomaly propagation before (after) lag 0.

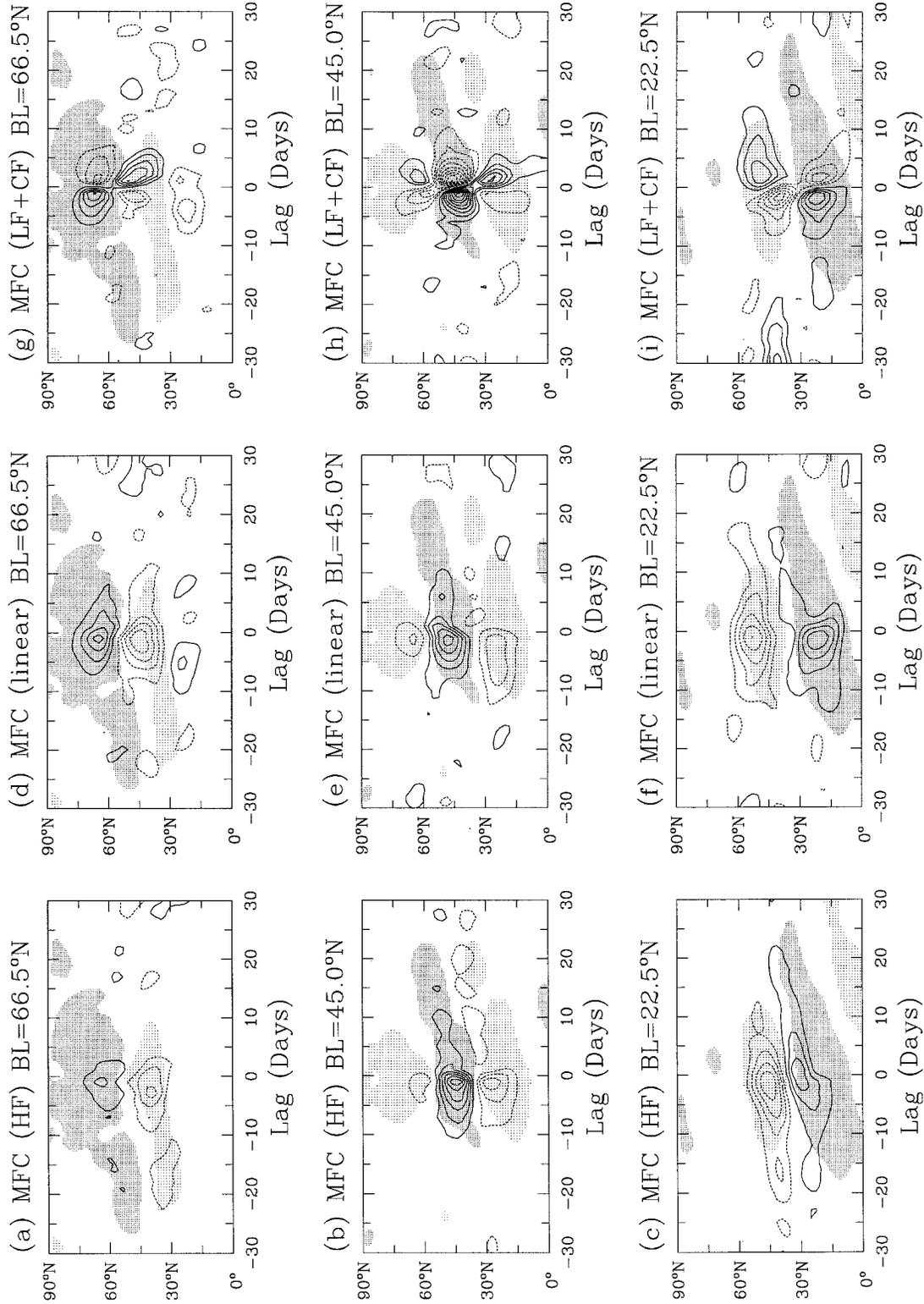The above decomposition also reveals that the anomalous HF eddy angular momentum flux convergence

FIG. 7. As Fig. 6, except for the NH winter. (d)–(f): The regressed anomalous eddy angular momentum flux convergence due to the linear (stationary − transient) terms; (g)–(i): The regressed anomalous summation of the low-frequency and cross-frequency eddy angular momentum flux convergence terms.

maintains its spatial structure for as long as 15 or 20 days, depending upon the latitude and season. This prolonged period of similar spatial structure for the anomalous HF eddy angular momentum flux convergence suggests that a positive feedback (James et al. 1994) may be taking place, that is, at subtropical latitudes the anomalous zonal mean flow changes the structure of the HF transient eddies in such a manner as to continually cause the zonal mean anomaly to propagate poleward, at high latitudes the zonal mean anomaly alters the structure of the HF transient eddies so as to maintain the zonal mean anomaly in a fixed position, and in midlatitudes both of the above processes take place. However, if this positive eddy–zonal mean feedback is indeed occuring, its influence must be relatively weak. This is because the anomalous *unfiltered* eddy angular momentum flux convergence (Figs. 4a–c, 5a–5c) undergoes substantial structural changes over a time period shorter than that of the existence of the HF eddy angular momentum flux convergence anomalies. This behavior just reflects the property that the decay of the M_R anomalies by the anomalous eddy angular momentum flux convergence is dominated by the summation of the LF and CF terms.

c. Eddy heat fluxes

We next examine the regression of the vertically integrated anomalous eddy heat flux (the integral extends from the lower boundary to 500 mb). When the anomalous eddy heat flux is decomposed into various frequency bands, in the same manner as the anomalous eddy angular momentum flux convergence, it is found that only the HF eddy heat fluxes have a coherent, organized spatial and temporal structure (see Figs. 8a–c for the NH winter and Figs. 8d–f for the SH summer). At all latitudes and seasons, one consistent property is that a poleward (equatorward) anomalous HF eddy heat flux coincides with a positive (negative) M_R anomaly (the region of statistically significant anomalous M_R is indicated by shading in Fig. 8). This relationship between the signs of the two anomalies is not surprising, since baroclinic instability theory implies an increase in the poleward anomalous HF eddy heat flux at the same latitude as enhanced surface baroclinicity, and although not calculated, one would normally expect a close relationship between the sign of the anomalous surface baroclinicity and anomalous M_R, because of thermal wind balance.

At each season and latitude, a poleward (equatorward) anomalous HF eddy heat flux occurs at the same latitude as the positive (negative) anomalous HF eddy angular momentum flux convergence. The signs of these anomalous fluxes can also be related to signs of anomalous Eliassen–Palm (Edmon et al. 1980) or wave activity flux; that is, since a poleward anomalous HF eddy heat flux corresponds to an anomalous upward wave activity flux, the sign of the anomalous HF eddy angular

momentum flux convergence implies that the direction of anomalous wave activity propagation is always away from the latitude of anomalous upward wave activity propagation. The opposite signs apply to equatorward anomalous HF eddy heat fluxes.

The above description of the HF wave activity fluxes indicates that wherever anomalous M_R is positive (negative), the anomalous wave activity flux is upward and outward (downward and inward). Because of the link between anomalous M_R and anomalous wave activity flux, it could be tempting to speculate that positive (negative) anomalous M_R coincides with episodes of enhanced (weakened) baroclinic lifecycles (Hoskins 1983). However, at a number of different seasons and latitudes, the anomalous HF eddy angular momentum flux convergence leads the anomalous HF eddy heat flux. This behavior is opposite to that which is expected for the classic baroclinic life cycle of numerical models, in which the initial state is wave free. However, one possible explanation for this behavior is that the surface friction changes the surface baroclinicity, after the anomalous HF eddy angular momentum flux convergence alters the M_R field.

d. Anomalous streamfunction

The anomalous horizontal circulation associated with the poleward-propagating M_R anomalies is investigated by examining the anomalous 300-mb streamfunction field. The aim of this analysis is both to show that a wide range of longitudes contributes to the M_R anomalies and to address the question of whether the M_R anomaly propagation is related to the dominant low-frequency anomalies such as the Pacific–North America and North Atlantic oscillation patterns (Wallace and Gutzler 1981). The anomalous 300-mb streamfunction is illustrated for various lags at the subtropical base latitudes for the NH winter (Fig. 9) and the SH summer (Fig. 10), as these base latitudes show prominent poleward M_R anomaly propagation. The poleward propagation is most easily visualized by noting which latitudes form the latitudinal boundaries of the main shaded region. Upon comparison of the anomalous streamfunction at lag $+3$ days relative to lag -9 days, one can see that both the northern and southern boundaries of this shaded region have moved poleward. However, in both hemispheres, this propagation does not take place at the longitudes where the anomalous streamfunction has its largest amplitude. For example, in the NH, the anomalous streamfunction amplitude is largest in the central North Pacific, yet most of the poleward propagation takes place in the Atlantic to European sector between between 45°W and 90°E. Furthermore, it is clear that these spatial patterns do not resemble the Pacific–North America and North Atlantic oscillation patterns.
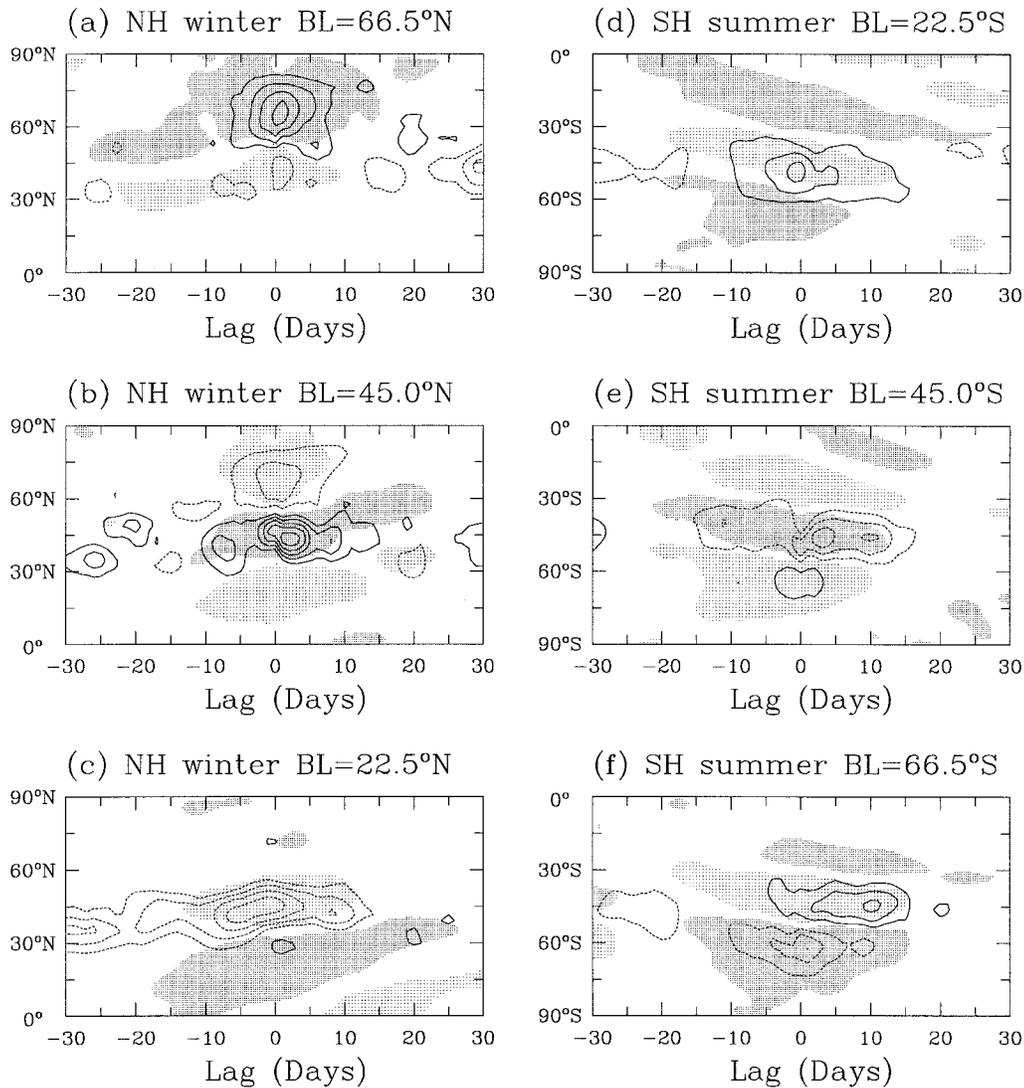
FIG. 8. Regressed anomalous HF eddy heat flux with base latitudes of (a) 66.5°N, (b) 45.0°N, and (c) 22.5°N for the NH winter, and (d) 22.5°S, (e) 45.0°S, and (f) 66.5°S for the SH summer. The contour interval is 0.1 K m s⁻¹. Solid contours are positive, dashed contours negative, and the zero contour is omitted. Shaded values correspond to the anomalous M_R values that exceed the 95% significance level, with dark (light) shading denoting positive (negative) t values.

4. Concluding remarks

This study presents the results of an analysis in which anomalous M_R at three base latitudes is regressed against various quantities. The main finding is that poleward propagation of M_R anomalies takes place in both hemispheres during both the winter and summer seasons. As the climatological Northern (Southern) Hemisphere winter (summer) are seasons of relatively large (small) stationary wave amplitude, such results imply that the existence of the poleward-propagating M_R anomalies is not sensitive to the presence or absence of large-amplitude stationary waves. Furthermore, the propagation speed of the M_R anomalies is larger and more uniform in the subtropical and high latitudes than in midlatitudes

where the propagation speed is close to zero for several days near the anomaly maximum. In addition, at high latitudes, equatorward M_R anomaly propagation was found to take place after poleward M_R anomaly propagation.

An examination of the angular momentum budget reveals that the M_R anomaly evolution is dominated by the anomalous eddy angular momentum flux convergence and the anomalous friction torque. The anomalous high-frequency eddy angular momentum flux convergence drives the poleward M_R anomaly propagation in the subtropics and midlatitudes. For the Northern Hemisphere, the anomalous eddy angular momentum flux convergence due to the interaction between stationary
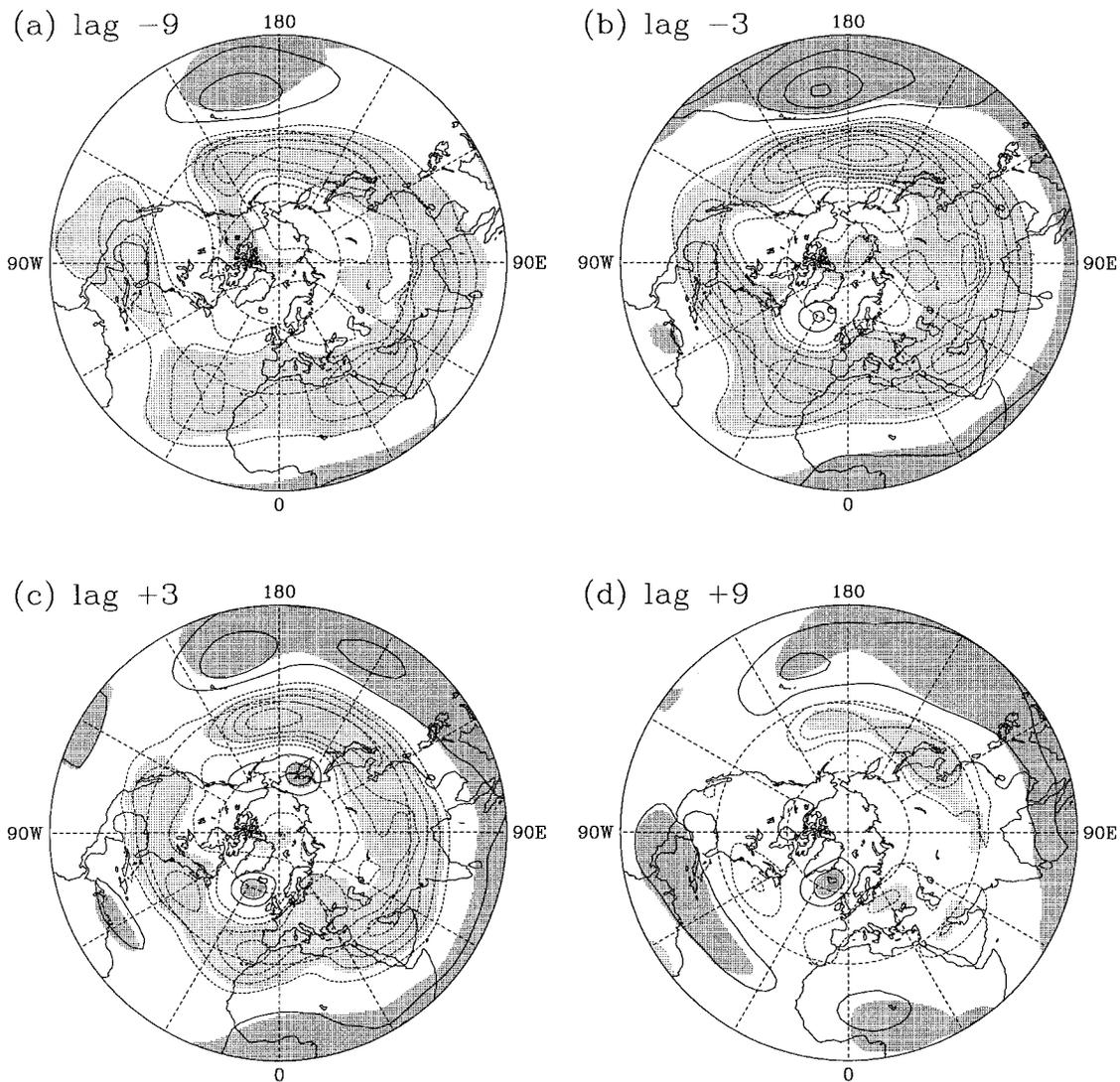
(a) lag −9

(b) lag −3

(c) lag +3

(d) lag +9

FIG. 9. Regressed anomalous 300-mb streamfunction at (a) lag −9 days, (b) lag −3 days, (c) lag +3 days, and (d) lag +9 days for a base latitude of 22.5°N for the NH winter. The contour interval is 1.0×10^6 m^2 s^{-1}. Solid contours are positive, dashed contours negative, and the zero contour is omitted. Shaded values exceed the 95% significance level, with dark (light) shading denoting positive (negative) t values.

and transient eddies also contributes to the poleward M_R anomaly propagation. On the other hand, in high latitudes of both hemispheres, it is the summation of the anomalous cross-frequency and low-frequency eddy angular momentum flux convergence that is the primary contributor to the M_R anomaly propagation.

The findings of this study suggest that the poleward M_R anomaly propagation is affected by a high-frequency transient eddy feedback. However, once the M_R anomaly attains its largest amplitude, the influence of this feedback is dominated by the summation of the cross-frequency and low-frequency eddy angular momentum flux convergence. Together with the anomalous friction torque, it is this summation of terms that accounts for the decay of the M_R anomalies.

One surprising finding in this study is the prominent

role played by both the cross-frequency and low-frequency eddy terms. The fact that these terms attain their largest amplitude several days after the HF eddy terms become well established hints at an upscale cascade to low-frequency as being important for the M_R anomaly evolution. However, this result does not refute the hypothesis proposed by James and Dodd (1996) that the poleward M_R anomaly propagation may result from wave–mean flow interaction in a manner analogous to sudden stratospheric warming.

(a) lag −9

(b) lag −3

(c) lag +3

(d) lag +9
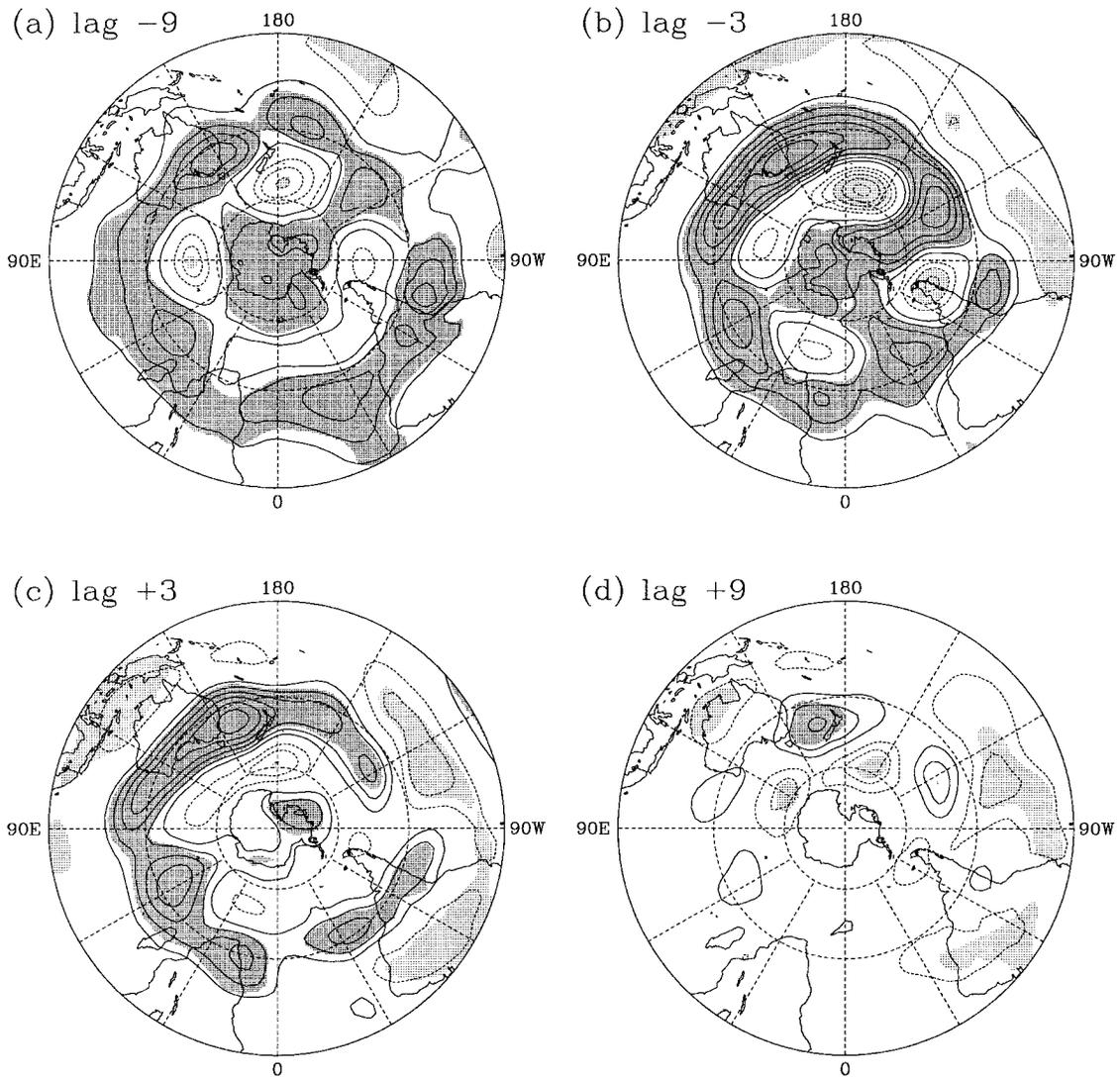
FIG. 10. As Fig. 9, except for a base latitude of 22.5°S for the SH summer.

REFERENCES

Davis, R., 1976: Predictability of sea surface temperature and sea level pressure anomaly over the North Pacific Ocean. *J. Phys. Oceanogr.,* **6,** 249–266.

Edmon, H. J., B. J. Hoskins, and M. E. McIntyre, 1980: Eliassen–Palm cross sections for the troposphere. *J. Atmos. Sci.,* **37,** 2600–2616.

Feldstein, S. B., and S. Lee, 1996: Mechanisms of zonal index variability in an aquaplanet GCM. *J. Atmos. Sci.,* **53,** 3541–3555.

Hartmann, D.L., 1995: A PV view of the zonal flow vacillation *J. Atmos. Sci.,* **52,** 2561–2576.

Hoskins, B. J., 1983: Modelling of the transient eddies and their feedback on the mean flow. *Large-Scale Dynamical Processes in the Atmosphere,* B. J. Hoskins and R. P. Pearce, Eds., Academic Press, 169–199.

James, I. N., and J. P. Dodd, 1996: A mechanism for the low-frequency variability of the mid-latitude troposphere. *Quart. J. Roy. Meteor. Soc.,* **122,** 1197–1210.

James, P. M., K. Fraedrich, and I. N. James, 1994: Wave-zonal-flow interaction and ultra-low-frequency variability in a simplified global general circulation model. *Quart. J. Roy. Meteor. Soc.,* **120,** 1045–1067.

Karoly, D. J., 1990: The role of transient eddies in low-frequency zonal variations of the Southern Hemisphere. *Tellus,* **42A,** 41–50.

Kidson, J. W., 1985: Index cycles in the Northern Hemisphere during the Global Weather experiment. *Mon. Wea. Rev.,* **113,** 607–623.

——, 1986: Index cycles in the Southern Hemisphere during the Global Weather Experiment. *Mon. Wea. Rev.,* **114,** 1654–1663.

——, 1988: Indices of the Southern Hemisphere zonal wind. *J. Climate,* **1,** 183–194.

Kutzbach, J., 1967: Empirical eigenvectors of sea level pressure, surface temperature, and precipitation complexes over North America. *J. Appl. Meteor.,* **6,** 791–802.

Lee, S., and S. B. Feldstein, 1996: Mechanisms of zonal index evolution in a two-layer model. *J. Atmos. Sci.,* **53,** 2232–2246.

Lyons, S. W., and B. Hundermark, 1992: Zonal-wind oscillations over the Western Hemisphere during winter: Further evidence of a zonal-eddy relationship. *Mon. Wea. Rev.,* **120,** 1878–1899.

Nigam, S., 1990: On the structure of variability of the observed tropospheric and stratospheric zonal-mean zonal wind. *J. Atmos. Sci.,* **47,** 1799–1813.

Pedlosky, J., 1970: Finite amplitude baroclinic waves. *J. Atmos. Sci.,* **27,** 15–30.

Riehl, T., C. Yeh, and N. E. LaSeur, 1950: A study of variations of the general circulation. *J. Meteor.,* **7,** 181–194.

Robinson, W., 1991: The dynamics of the zonal index in a simple model of the atmosphere. *Tellus,* **43A,** 295–305.

——, 1996: Does eddy feedback sustain variability in the zonal index? *J. Atmos. Sci.,* **53,** 3556–3569.

Simmons, A. J., and B. J. Hoskins, 1978: The life cycles of some nonlinear baroclinic waves. *J. Atmos. Sci.,* **35,** 414–432.

Wallace, J. M., and D. S. Gutzler, 1981: Teleconnections in the geopotential height field during the Northern Hemisphere winter. *Mon. Wea. Rev.,* **109,** 784–812.

Weickmann, K. M., and P. D. Sardeshmukh, 1994: The atmospheric angular momentum cycle associated with a Madden–Julian oscillation. *J. Atmos. Sci.,* **51,** 3194–3208.

——, G. N. Kiladis, and P. D. Sardeshmukh, 1997: The dynamics of intraseasonal atmospheric angular momentum oscillations. *J. Atmos. Sci.,* **54,** 1445–1461.

Yu, J. Y., and D. L. Hartmann, 1993: Zonal flow vacillation and eddy forcing in a simple GCM of the atmosphere. *J. Atmos. Sci.,* **50,** 3244–3259.